Zeitschrift für anorganische und allgemeine Chemie

Journal of Inorganic and General Chemistry
ZAAC
Zeitschrift für anorganische und allgemeine Chemie

RESEARCH ARTICLE OPEN ACCESS

Tuning the Photochemistry of Entatic State Model Systems

Alexander Hoffmann[1] | Julia Stanek[1] | Stefan Hofmann[2] | Michael Rampp[2] | Benjamin Maerz[2] | Benjamin Grimm-Lebsanft[3,4] | Melissa Kindler[3,4] | Tobias Seitz[1] | Michael Rübhausen[3,4] | Wolfgang Zinth[2] | Sonja Herres-Pawlis[1]

[1]Institute of Inorganic Chemistry, RWTH Aachen University, Aachen, Germany | [2]Institute for BioMolecular Optics and Center for Integrated Protein Science (CIPSM), Faculty of Physics, Ludwig-Maximilians-Universität Munich, Munich, Germany | [3]Institute of Nanostructure and Solid State Physics, University of Hamburg, Hamburg, Germany | [4]Center for Free-Electron Laser Science (CFEL), Hamburg, Germany

Correspondence: Alexander Hoffmann (alexander.hoffmann@ac.rwth-aachen.de) | Wolfgang Zinth (wolfgang.zinth@physik.uni-muenchen.de) | Sonja Herres-Pawlis (sonja.herres-pawlis@ac.rwth-aachen.de)

Received: 12 December 2025 | **Revised:** 27 February 2026 | **Accepted:** 10 March 2026

Keywords: copper complexes | entatic state | excited states | guanidine | time-resolved spectroscopy

ABSTRACT

The entatic state model system, the copper guanidinoquinoline complex pair $[Cu(DMEGqu)_2]^{+/2+}$, was herein studied regarding its photo-dynamics upon excitation. The photo-induced excited states of the copper(I) complex were investigated with time-resolved infrared and UV/Vis absorption spectroscopy, yielding the excited states' time constants upon metal-to-ligand charge transfer. Additional density functional theory calculations yield insights into the electronic structures of these excited states. The combined theoretical and experimental approach was used to construct the schematic reaction pathway of the excited states of $[Cu(DMEGqu)_2]PF_6$. Further, using a previous study of an entatic state model complex with a different guanidine moiety, $[Cu(TMGqu)_2]PF_6$, the substituents' effects on the complex cation's photo-dynamics were evaluated. The comparison shows that the less bulky and more rigid DMEG moiety measurably affects the charge transfer dynamics, underscoring the entatic state model as a potential tool for controlling copper photochemistry.

1 | Introduction

A detailed understanding of chemical processes of photoexcited transition metal complexes, including copper complexes, is crucial for the development of modern applications, i.e., dye sensitized solar cells, organic light emitting diodes (OLEDs), and photocatalysis [1–6]. While promising, the application of early transition metals in these areas is challenging due to their short lifetimes, caused by a combination of factors like insufficient ligand-field splitting or structural flattening [7, 8]. To overcome these limitations, the elucidation of structure–property relationships regarding the time constants of the different emerging excited states is the focus of current research [9–11]. Hereby, the reaction pathway of the photoexcitation of a copper complex is studied with focus on its various excited states and their corresponding lifetimes. Cu(I) complexes are promising systems for the development of late transition metal photosensitizers due to their potentially long-lived excited states [12–16]. These copper complexes often contain sterically demanding N-donor ligands which control the time constants of internal conversion (IC) and intersystem crossing (ISC). The basic $[Cu(dmp)_2]^+$ system (dmp = 2,9-dimethyl-1,10-phenanthroline), for example, exhibits shorter time constants of the charge-separated singlet and triplet states than the functionalized analogs with bulkier substituents [9, 17–24]. In contrast, the excited states of the herein studied entatic state model system possess extraordinarily short time constants. The IC and ISC processes in the entatic state proceed distinctly faster than for the bulkier diimine system [25].

The entatic state principle was developed by Vallee and Williams in the 1960s [26, 27]. It was defined as the impact of the protein surrounding or the ligand sphere on the structure and/or reactivity of the active site of a protein or a complex. An early explanation for the fast electron transfer processes facilitated by type-I Cu proteins

Dedicated to Prof. Peter Klüfers on the occasion of his 75th birthday.

[27, 28], the study of the entatic state has resulted in a broad range of reported coordination compounds as entatic state model systems [29–36]. Over the years, the concept's definition saw intensive discussion and modifications [37–40]. For example, Comba et al. describe the entatic state as "the energization due to a misfit" between ligand and metal center or between system fragments of catalyst and substrate and the reactive complex [41]. Nowadays, the concept "entasis" comprises not only the energization induced by steric hindrance but also the electronic influence of certain donors on the metal center and the impact of the interaction with the reaction environment [41–43]. A system in its entatic state is stabilized in an energized form, which resembles the transition state of the reaction [41]. Thereby, the activation barrier and reorganization energy of the reaction are lowered and in case of the photoexcitation IC and ISC are accelerated [25]. This effect of the entatic state was determined for the copper guanidinoquinoline complex $[Cu(TMGqu)_2]PF_6$ with TMGqu (1,1,3,3-tetramethyl-2-(quinolin-8-yl)guanidine) as ligand. This complex and its Cu(II) counterpart were previously reported as model systems for the geometric entatic state (Figure 1) [44]. The Cu(I) and Cu(II) complexes possess strong structural resemblance, both highly distorted from either ideal coordination polyhedron (tetrahedron for Cu(I) and square planar for Cu(II)) [45]. $[Cu(TMGqu)_2]PF_6$ follows a pathway of various excited states after photoexcitation which were characterized by different time-resolved spectroscopic methods, yielding three relatively short-lived, "entatic" MLCT (metal-to-ligand charge–transfer) states. An internal conversion of S_1 to a flattened $S_{1,relax}$ state and the following ISC to T_1 and back to S_0 have very small time constants compared to diimine systems in literature [23, 25]. The initial study of $[Cu(TMGqu)_2]PF_6$ was therefore able to correlate the entasis of a copper compound to its photo-dynamics. The specific ligand features of the guanidine unit are based on the outstanding donor properties and the high basicity of those systems [46]. Guanidine donors act as ligands in various applications, e.g., bioinorganic chemistry [46–57] and polymerization catalysis [58–68].

Herein, we discuss the determination of the excited state dynamics of $[Cu(DMEGqu)_2]PF_6$ (DMEGqu: 1,3-dimethyl-*N*-(quinolin-8-yl)imidazolidin-2-imine, Figure 1) after photoexcitation. The structural and electronic properties of different MLCT states were examined via transient absorption and IR spectroscopy and DFT (density functional theory) calculations. The influence of the more rigid guanidine system compared to the TMGqu system is elucidated regarding the entatic state principle in the excited states. Taking into account the electron-transfer in the ground state, the DMEGqu system already reveals a significant deceleration in comparison to the TMG parent system owing to both the larger structural change upon oxidation and the more rigid DMEG moiety.

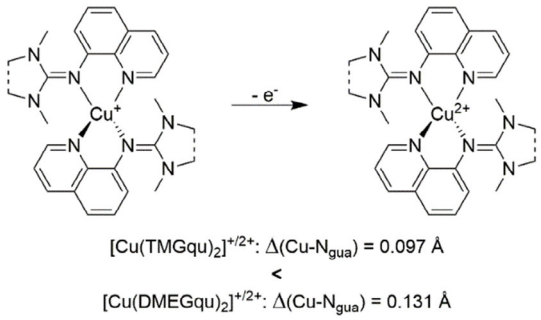

FIGURE 1 | Schematic description of the differently pronounced structural change during the electron transfer of $[Cu(TMGqu)_2]^{+/2+}$ or $[Cu(DMEGqu)_2]^{+/2+}$; $\Delta(Cu\text{-}N_{gua})$: difference in $Cu\text{-}N_{gua}$ bond length between the Cu^+ and Cu^{2+} structures. TMGqu is 1,1,3,3-tetramethyl-2-(quinolin-8-yl)guanidine) (only solid lines) and DMEGqu is 1,3-dimethyl-N-(quinolin-8-yl)imidazolidin-2-imine (solid and dashed lines).

2 | Results and Discussion

Given the electronic similarity between the MLCT states and the Cu(II) state, both oxidation states of the $[Cu(DMEGqu)_2]^{+/2+}$ redox couple were initially examined via static IR and UV/Vis absorption spectroscopic methods (Figure 2). Despite the geometric similarities of both complex cations (Figure 2, left), there are distinct differences in the characteristic spectral features of Cu(I) and Cu(II) complexes. These differences arise from their deviating electronic structures, which allow for the construction of static difference spectra that can be later compared to those of the excited Cu(I) complex. The infrared spectra of both oxidation states show intense bands of typical guanidine and quinoline vibrations (Figure 2, middle) which respond sensitively to oxidation state changes. The absorption spectra of the Cu(I) and Cu(II) complexes depict intense transitions in the visible region. For the Cu(I) complex $[Cu(DMEGqu)_2]^+$, said transition is located at approximately 430 nm and can be attributed to a $Cu \rightarrow \pi^*$

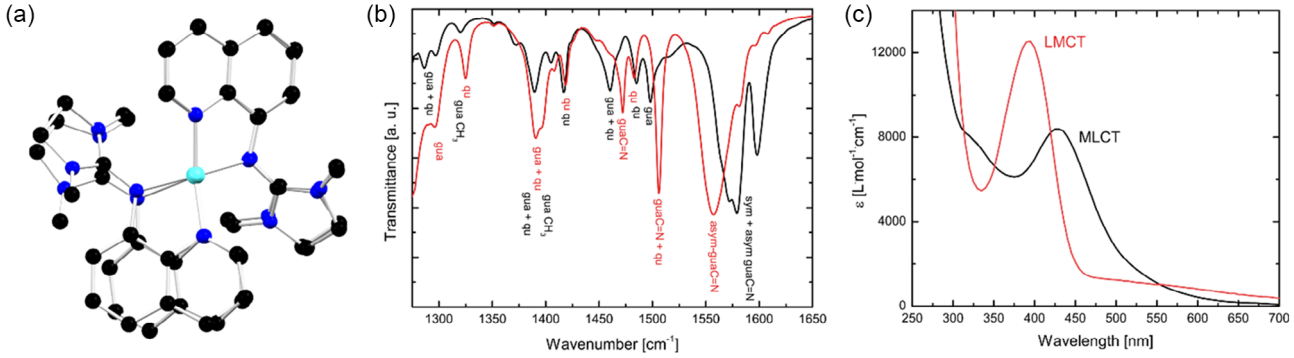

FIGURE 2 | **Left**: Overlay of the molecular structures in the solid state of the complex cation pair $[Cu(DMEGqu)_2]^{+/2+}$; **middle**: Static infrared spectra of $[Cu(DMEGqu)_2]^+$ (black) and $[Cu(DMEGqu)_2]^{2+}$ (red) in CH_2Cl_2; **right**: static UV/Vis spectra of $[Cu(DMEGqu)_2]^+$ (black) and $[Cu(DMEGqu)_2]^{2+}$ (red) in CH_3CN.

metal-to-ligand charge transfer (MLCT). For $[Cu(DMEGqu)_2]^{2+}$, the transition at 390 nm is likewise attributed to a charge transfer, specifically the opposite $\pi^* \rightarrow Cu$ ligand-to-metal charge transfer (LMCT, Figure 2, right). Based on the information obtained from the ground state spectra, structural and electronic properties can be assigned to emerging excited states.

The excited state dynamics of the Cu(I) complex $[Cu(DMEG)_2]PF_6$ were examined using transient absorption and IR spectroscopy within a time interval of ~500 ps after photoexcitation. The corresponding fit amplitudes (Figure 3) contain information on the related reactions. Transient IR spectroscopy [69–71] was conducted to evaluate the temporal change of the typical ligand vibrations after photoexcitation of $[Cu(DMEGqu)_2]PF_6$ and compare them to those of the previously studied $[Cu(TMGqu)_2]PF_6$ [25]. The measurements were performed in dichloromethane (CH_2Cl_2) with an excitation wavelength λ_{exc} of 400 nm. Figure 3 depicts the transient spectra at different delay times, and the decay-associated difference spectra (DADS) at certain decay times determined from the global fit. These spectra allow the molecular interpretation of the responsible states for the observed decay processes. The transient infrared spectra measured at the beginning indicate that the initial ground state absorption disappears upon excitation and another species with Cu(II) character appears. The dotted curve in Figure 3, middle, is the inverted ground-state absorption spectrum of the initial sample. A comparison of the negative bands in the DADS with the static absorption spectrum of the two DADS (middle and bottom) clearly shows that a similar amount of ground-state population recovers with the two processes. This observation supports the interpretation given below that state $S_{1,relax}$ decays via two channels of equal efficiency, i.e., $\tau_{2a} = \tau_{2b}$. Three time constants were obtained via global modeling ($\tau_2 = 4 \pm 0.8$, $\tau_3 = 15 \pm 1$, and $\tau_4 = 360 \pm 20$ ps; Table 1). Since the spectra related to τ_2 and τ_4 and the ground state spectrum of $[Cu(DMEGqu)_2]^{2+}$ depict very similar vibrations, the excited states are identified as MLCT species with Cu(II) character. A comparison of the spectra of τ_3 and the ground state spectrum of S_0 shows red-shifted vibration bands of the excited state, which indicates a cooling of a vibrationally excited, hot ground state [72]. The DADS at 360 ps shows very high agreement with the ground state FTIR difference spectra of $[Cu(DMEGqu)_2]^{+}$ and $[Cu(DMEGqu)_2]^{2+}$ (dotted black line, Figure 3, bottom). Thus, an almost complete regeneration of the $[Cu(DMEGqu)_2]^{+}$ ground state appears. Therefore, only a small percentage of long living excited species (exciplex, vide infra) is present.

Similar results are received via transient absorption spectroscopy in the UV/Vis region (Figure 4, Table 1). The amplitudes of the transient difference spectra show a reduction by ~50% during the first 5 ps, after which a decay on the 100 ps timescale takes over. The global modeling of the spectra, obtained from the

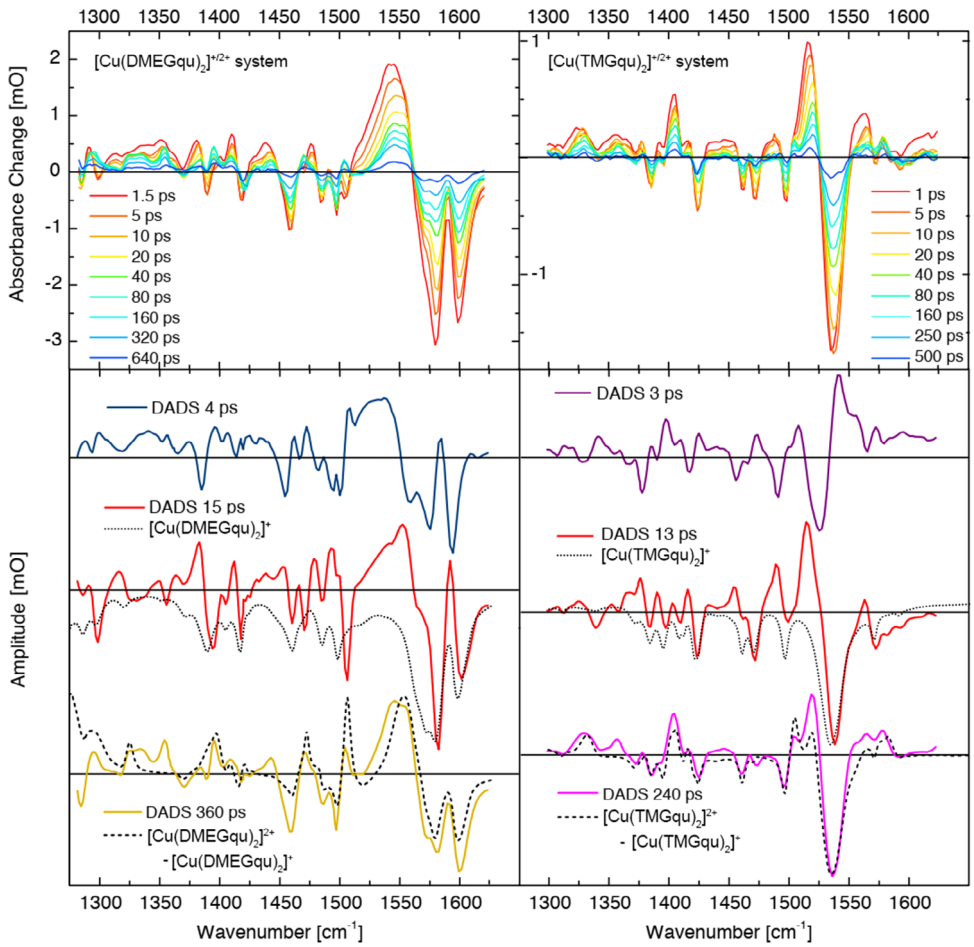

FIGURE 3 | Transient MIR difference spectra of $[Cu(DMEGqu)_2]PF_6$ (left) and $[Cu(TMGqu)_2]PF_6$ (right) in CH_2Cl_2 for selected delay times (excitation at 400 nm) and decay-associated difference spectra (DADS) for selected decay times of $[Cu(DMEGqu)_2]PF_6$ (left) and $[Cu(TMGqu)_2]PF_6$ (right) in CH_2Cl_2. The dotted curves represent the inverted ground-state absorption spectra of the initial sample and the dashed curves the difference spectra.

TABLE 1 | Overview of decay times for the optical excitation of $[Cu(TMGqu)_2]PF_6$ [25] and $[Cu(DMEGqu)_2]PF_6$.

		$[Cu(DMEGqu)_2]^+$		$[Cu[TMGqu)_2]^+$	
		CH_2Cl_2	CH_3CN	CH_2Cl_2	CH_3CN
TR-IR				$\lambda_{pump} = 400$ nm	
	τ_2 [ps]	4 ± 0.8	n.d.	3 ± 1	2 ± 1.5 [25]
	τ_3 [ps]	15 ± 1	n.d.	13 ± 1	11 ± 3 [25]
	τ_4 [ps]	360 ± 20	n.d.	240 ± 20	120 ± 20 [25]
TR-UV/Vis				$\lambda_{pump} = 400$ nm	
	τ_1 [ps]	0.3 ± 0.3	0.3 ± 0.2	0.7 ± 0.5	0.3 ± 0.2
	τ_2 [ps]	2.6 ± 1	1.4 ± 0.4	1.8 ± 1	1.4 ± 0.2
	τ_3 [ps]	15 ± 4	23 ± 10	14 ± 3	9 ± 3
	τ_4 [ps]	400 ± 30	170 ± 20	260 ± 20	115 ± 10

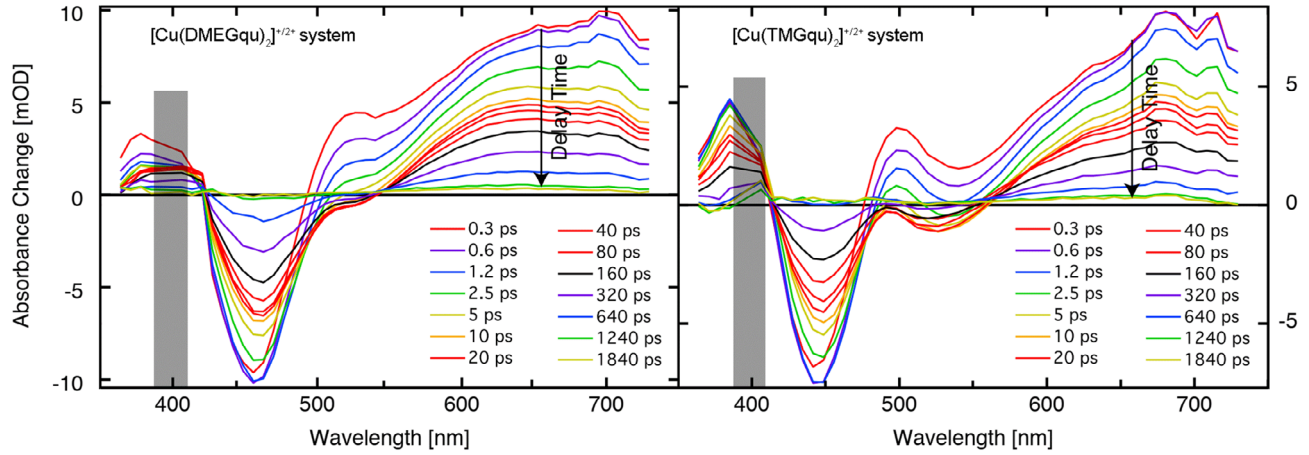

FIGURE 4 | Transient UV/Vis difference spectra of $[Cu(DMEGqu)_2]PF_6$ (left side) and $[Cu(TMGqu)_2]PF_6$ (right side) in CH_2Cl_2 for selected delay times. The gray area indicates the spectral range where the excitation pulse influences the detected absorption data.

measurements in CH_2Cl_2 with $\lambda_{exc} = 400$ nm, results in four time constants ($\tau_1 = 0.3 \pm 0.3$, $\tau_2 = 2.6 \pm 01$, $\tau_3 = 15 \pm 4$, and $\tau_4 = 400 \pm 30$ ps). The three longer living values are similar to the time constants from transient IR spectroscopy. After photoexcitation, a decrease in the Cu(I) absorption at 430 nm is observed. Concurrently, an increase of the absorption at 390 nm is detected, indicating the development of a Cu(II) species (see Figure S1). Additionally, a broad absorption at 500–700 nm arises, which can be assigned to the formation of a quinolinyl radical [73]. These absorption bands of the transient species vanish completely after a reaction time of 1000–3000 ps and the Cu(I) absorptions are regenerated.

The transient UV/Vis spectroscopic measurements were also performed with an excitation wavelength of 320 nm. Their analysis yields four time constants, calculated via global modeling, that are of similar values as the constants obtained at $\lambda_{exc} = 400$ nm, which is in agreement with the previous study of the $[Cu(TMGqu)_2]PF_6$ system [25]. Therefore, the excitation wavelength has only minimal influence on the type and lifetime of the arising excited states.

The comparison of the transient spectra shows that the two systems $[Cu(TMGqu)_2]PF_6$ and $[Cu(DMEGqu)_2]PF_6$ exhibit similar spectral behavior (Table 1, Figures 3 and 4). The time constants τ_1 to τ_3 are of similar size, but the lifetimes of the DMEGqu-coordinated species are slightly longer. Only the T_1 state with lifetime τ_4 is considerably more stable for $[Cu(DMEGqu)_2]PF_6$ (see Figure 5 showing a direct comparison at a probing wavelength of 659.6 nm).

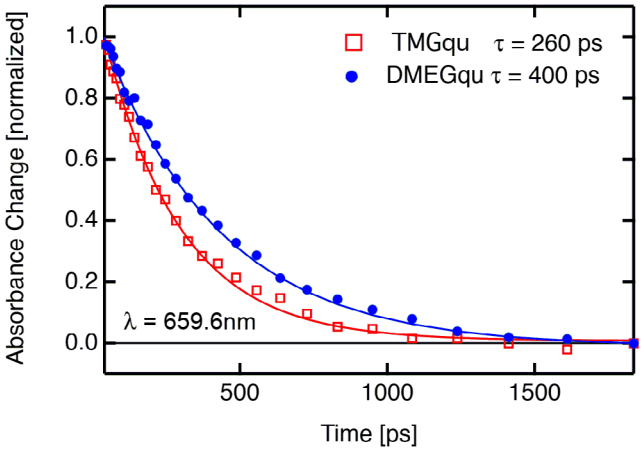

FIGURE 5 | Comparison of the lifetimes of the longest-living state of $[Cu(TMGqu)_2]PF_6$ (red, 260 ps) and $[Cu(DMEGqu)_2]PF_6$ (blue, 400 ps) in CH_2Cl_2 determined via transient UV/Vis spectroscopy @ 659.6 nm. Absorption data are normalized and off-set corrected.

The change of the solvent from CH_2Cl_2 to acetonitrile (CH_3CN) exhibits a distinct impact on the time constant of the excited states, while the character and spectroscopic features of the arising species remain constant. The time constants of the flattened ^{3}MLCT-state decay are systematically shorter in acetonitrile than in CH_2Cl_2. The excited states are destabilized in the more polar solvent (CH_3CN). The influence of the solvent may be caused by the formation of exciplex species, which are formed by a loose solvent coordination [24, 74, 75]. Moreover, in the DMEG case, the anion may have a stronger contact to the formal Cu(II) ion [76] in the exciplex which additionally stabilizes its lifetime. With the information obtained from the experiments and DFT calculations, a reaction pathway of the excited states was derived (Figure 6). Thereby, spectroscopic and structural properties and time constants are referred to as defined excited state species.

With the excitation of the Cu(I) ground state S_0 with a defined wavelength λ_{exc}, an electron is transferred from the metal center to the ligand sphere and an λ_{exc}-dependent excited state S_{19} (Franck-Condon state with MLCT character) is populated, which decays to S_1 on a fast femtosecond timescale following Kasha's rule. According to Kasha's rule, fluorescence or phosphorescence originates from the electronically lowest excited state of a given multiplicity [77]. Hence, an excited species with Cu(II) character arises with the time constant τ_1, which is defined as ^{1}MLCT $S_{1,relax}$ state. This singlet state possesses structural (Table 2) and spectroscopic features similar to the ground state $[Cu(DMEGqu)_2]^{2+}$ and additionally shows UV/Vis absorptions of a ligand (quinolinyl) radical. In the following, the $S_{1,relax}$ decays with $\tau_2 = 1.4$ ps (value for acetonitrile). Approximately 50% reach the triplet ^{3}MLCT state via ISC with the time constant τ_{2a}. The structural and spectroscopic properties of T_1 resemble $S_{1,relax}$ and the Cu(II) ground state. The remaining population of the flattened ^{1}MLCT follows another decay channel to a hot ground state (detected by TR-IR, τ_{2b}), which

TABLE 2 | Optimized excited singlet state geometry data and the triplet state geometry.

	GS-Cu(I)	GS-Cu(II)	$S_{1,relax}$	S_{19}	T_1
Cu–N_{gua} [Å]	2.166	2.065	2.063	2.076	1.987
Cu–N_{qu} [Å]	2.041	2.086	2.059	2.072	1.974
Cu–N_{gua2} [Å]	2.166	2.065	2.063	2.076	1.987
Cu–N_{qu2} [Å]	2.041	2.086	2.059	2.072	1.974
∡ CuN_2-CuN'_2	72.4	46.6	42.7	49.2	44.7

itself decays to S_0 with τ_3. We also tried to obtain emission spectra from the Cu(I) complex but obtained only emission spectra of the ligand (see SI, Figures S2 and S3).

The triplet state T_1 has a lifetime τ_4. It may form the ground state S_0 directly via another ISC by a back transfer of the electron from the formally reduced ligand to the copper ion with a rate of $1/\tau_{4a}$. A minor fraction of the T_1-population decays to the ground-state via an exciplex on the nanosecond time scale with the rate of $1/\tau_{4b}$. The time constant τ_4 (170 ps for $[Cu(DMEGqu)_2]PF_6$ in acetonitrile) is extremely short for the decay of an excited triplet state. In comparison, the T_1 species of substituted copper phenanthroline complexes possess time constants up to the ns time scale [12–16]. Additionally, τ_1 and τ_2 are distinctly faster than comparable time constants of copper complexes in the literature.

These fast decay times are promoted by the entatic state principle. The preflattened geometry and small structural differences between both the oxidation and the excited states of the complex promote a fast interconversion from S_{19} to S_1 and ISC to T_1 and back to S_0.

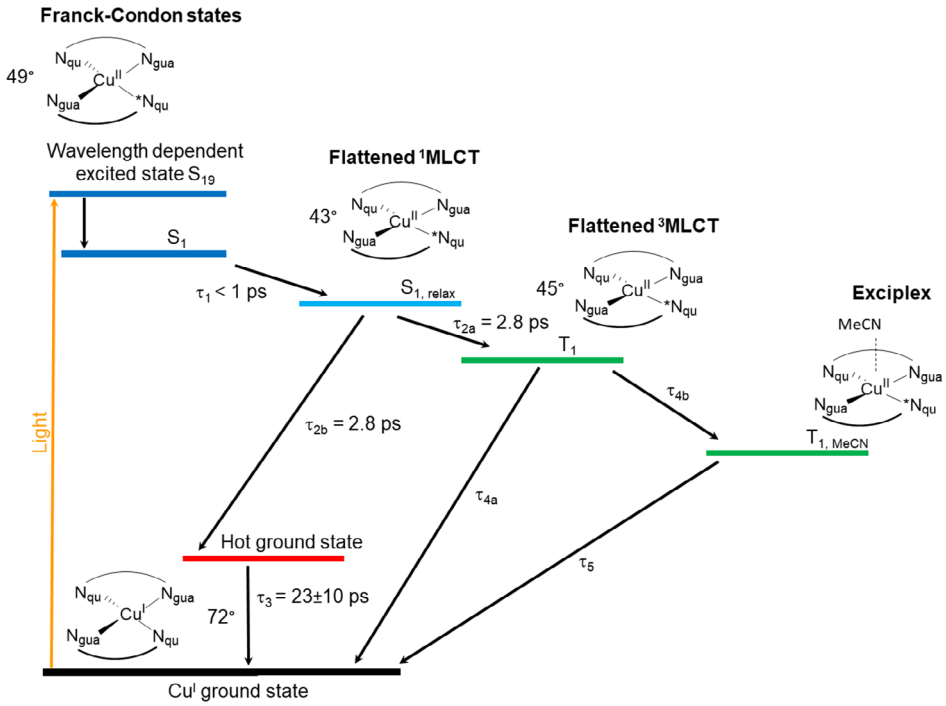

FIGURE 6 | Schematic reaction pathway of the excited states of $[Cu(DMEGqu)_2]^+$ in CH_3CN after photoexcitation. TD DFT calculations allow an assignment of the geometry of the excited states.

During the structural reorganization, the angle between the chelate planes on the one hand and the Cu–N_{gua} bond length on the other hand have to be changed leading to the corresponding orbital rotation required for an efficient spin–orbit coupling [76].

Remarkably, a comparison of the time constants of the excited states of $[Cu(DMEGqu)_2]PF_6$ with the values of $[Cu(TMGqu)_2]PF_6$ shows a deceleration of the decays of the excited species. Exemplarily, the time constant τ_4 increases from ca. 115 ps ($[Cu(TMGqu)_2]PF_6$) to 170 ps ($[Cu(DMEGqu)_2]PF_6$) in CH_3CN and from 260 to 400 ps in CH_2Cl_2, respectively (data from transient UV/Vis spectroscopic measurements). The slightly larger geometric difference of the $[Cu(DMEGqu)_2]^{+/2+}$ system enlarges the structural change during the process of photoexcitation. This influence of guanidine substituents on the properties of a complex as entatic state model system has already been discussed in terms of spectroscopic features [44, 76] and intermolecular electron transfer properties: The DMEG unit of the dimethylethylguanidinoquinoline (DMEGqu) ligand shows a slightly more rigid and slim structure in comparison to the TMG units of the TMGqu system, stronger affecting the structures of the corresponding copper complexes (Figure 1) [78, 79]. As a consequence, the $[Cu(DMEGqu)_2]^{+/2+}$ couple exhibits larger structural differences between the Cu(I) and Cu(II) states that reflect the structural changes in the MLCT states. This can be quantified by the more pronounced change of the geometric parameters, e.g., the Cu–N_{gua} bond length and the CuN_2–CuN_2' angle, obtained from molecular structures in the solid state [76]. In the DMEGqu species, the excited state species have to overcome a larger structural change (CuN_2–CuN_2' angle) during the IC and ISC processes, which increases the lifetimes of the individual excited states. Therefore, in $[Cu(DMEGqu)_2]^{+/2+}$, the entatic state influences the photoexcited reaction processes to a smaller extent than in the $[Cu(TMGqu)_2]^{+/2+}$ system. This can be well correlated with the smaller electron self-exchange rate constants of the $[Cu(DMEGqu)_2]^{+/2+}$ system [78, 79]. Additionally, due to a larger reorganization energy in nitrile solvents, the electron self-exchange rate of $[Cu(DMEGqu)_2]^{+/2+}$ is decelerated in contrast to $[Cu(TMGqu)_2]^{+/2+}$ [78, 79]. This is again in fine accordance with the charge–transfer data presented here.

The DFT calculations help to understand the vibronic behavior of the two complex pairs: The parent complex $[Cu(TMGqu)_2]PF_6$ shows an optical transition at 3.4 eV (365 nm) corresponding to a MLCT transition whereas the corresponding Cu(II) complex shows a complementary LMCT transition [44]. In the corresponding Raman spectra, a Cu–N bond length elongation and Cu distortion vibration at around 800 cm^{-1} (Cu(I): 778 and 811 cm^{-1}; Cu(II): 790 and 815 cm^{-1}) come into resonance at this excitation wavelength [44]. This vibronic mode geometrically connects the Cu(I) and the Cu(II) complex by combining the optical charge–transfer excitation with the distortion of the system along the reaction coordinate. This mode provides a charge-separated state which resembles the transition state of the inner-sphere electron transfer.

In the $[Cu(DMEGqu)_2]^{+/2+}$ system, the corresponding vibronic mode looks quite different. In both systems, DFT analysis reveals a MLCT in the Cu(I) complexes (see Figure 7, left, electron density difference map: EDDM) and an LMCT for the corresponding Cu(II) complexes (see Figure 7, right). But the compositions of the transitions are different: In the $[Cu(TMGqu)_2]^{+/2+}$ system, the MLCT purely consists of contributions from Cu d_{z2} to the π* of the quinoline transition and the LMCT contributions from π of the quinoline and the guanidine system to the Cu d

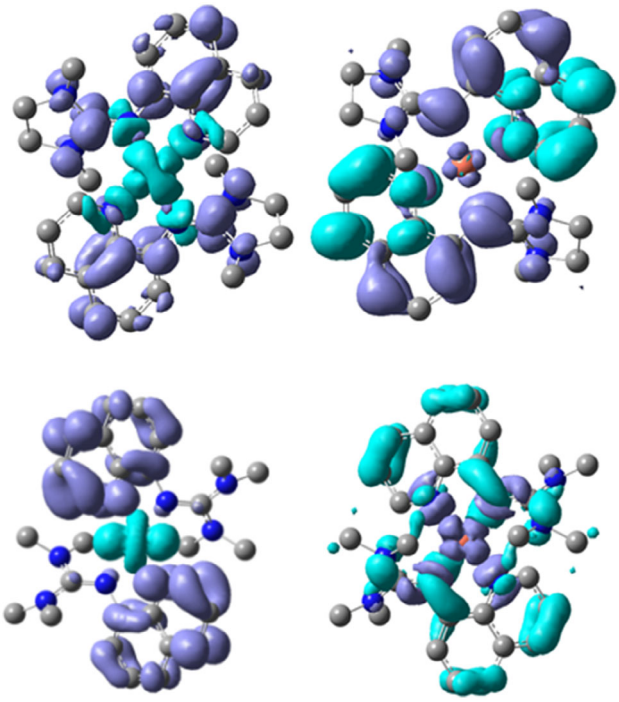

FIGURE 7 | Electron density difference map (EDDM) of the $[Cu(DMEGqu)_2]^{+/2+}$ (above) and the $[Cu(TMGqu)_2]^{+/2+}$ system [44] (bottom); on the left side: MLCT transitions and on the right side: LMCT transitions (light to dark).

transition [44]. However, in the $[Cu(DMEGqu)_2]^{+/2+}$ system, the MLCT consists of contributions from the Cu d orbital and the guanidine N donor to the π* system of the quinoline and the DMEG unit. The LMCT shows transitions from the π system of the quinoline to the Cu d orbital and the guanidine system. The contribution of the guanidine moiety in DMEGqu is explained by the MO scheme. In the TMGqu system the π orbitals of the quinoline and the guanidine moiety are separated whereas these orbitals partially mix in the DMEGqu system [76, 80].

3 | Conclusions

We investigated the influence of the different guanidine moieties of Cu(I) and Cu(II) complexes on the entatic state principle and their photochemistry. Complementary time-resolved techniques deliver lifetimes of the different excited states and, together with DFT studies, insights into the charge–transfer processes of the complexes. The comparison of the transient spectra of the different systems (complexes with the ligand TMGqu and DMEGqu) yields similar spectral behavior whereas the lifetimes with the DMEGqu ligand are longer which points to the notion that the involved species and the reaction scheme are highly similar. Nevertheless, the lifetimes of the flattened ^{3}MLCT-states show a pronounced ligand dependency: The guanidine moiety in DMEGqu is more rigid which impacts the regarded Cu complexes. The structural difference between the Cu(I) and the Cu(II) complexes is more pronounced than in the complexes with TMGqu, increasing the lifetimes of the excited states. The less pronounced entatic state of $[Cu(DMEGqu)_2]^{+/2+}$ compared to its $[Cu(TMGqu)_2]^{+/2+}$ counterpart therefore also affects the corresponding photodynamics of the Cu(I) complex. The

small changes in the different guanidine moieties of the ligands result in different electronic properties, enabling the engineering of the time constants by entatic state effects. Moreover, it shows that tuning of charge–transfer processes and electron transfer processes are inherently linked in guanidine copper complexes.

4 | Experimental Section

4.1 | Materials

All experiments involving air- and moisture-sensitive compounds were performed under N_2 atmosphere, purified with granulated P_4O_{10}, by Schlenk techniques or in a glovebox. The solvents (CH_3CN and CH_2Cl_2) were purified by distillation from CaH_2. The complexes ($[Cu(DMEGqu)_2]PF_6$ and $([Cu(DMEGqu)_2](PF_6)_2$ were prepared according to the literature [76].

4.2 | Transient IR and UV/Vis Absorption Spectroscopy

The ultrafast absorption changes were recorded using the pump-probe technique. Femtosecond pulses are generated by a Ti: Sapphire laser-amplifier system with a repetition rate of 1 kHz (Spitfire Pro, Tsunami, Spectra Physics) [81]. The pulses (central wavelength 800 nm, pulse duration 90 fs) are split into a pump pulse for excitation and a probe part to monitor the response of the excited sample.

4.2.1 | Excitation

For most of the experimental investigations, the pump pulse is obtained by frequency doubling the fundamental of the Ti: Sapphire laser-amplifier system to 400 nm. For the experiments with excitation at 320 nm, the pump pulses are generated by frequency doubling of 640 nm pulses produced in a home-built two-stage noncollinear optical parametric amplifier (NOPA) [82]. The excitation pulses are delayed relative to the probe pulse with a mechanical delay stage. Every second excitation pulse is blocked by a mechanical chopper to improve referencing.

4.2.2 | Probing in the Visible and Near UV

Broadband probing light was generated via a femtosecond white light super continuum (SC) and a spectral range extending from 320 to 720 nm was used. For SC light generation, a small portion of the 800 nm fundamental pulse was focussed on a CaF_2 plate [83]. The SC pulse is imaged on the sample with a diameter ~70 µm. The spectrum of the transmitted light is recorded for each pulse with a home-built spectrometer (detector array S3902-512Q from Hamamatsu). The measurements are performed under magic angle conditions and at room temperature. The excitation pulses (energy ca. 400 nJ) had a diameter of 210–250 µm for 400 nm excitation and 170 µm for 320 nm excitation. The instrumental response function had a duration (FWHM) of 100–150 fs.

4.2.3 | Probing in the Mid-IR

Generation of the mid-IR probe pulses (1275–1630 cm^{-1}) uses a combination of a non-collinear [84, 85] and a collinear optical parametric amplifier to generate a pair of intense pulses in the near IR at around 1.4 and 1.8 µm. Difference frequency mixing of these two pulses in an $AgGaS_2$ nonlinear crystal allows to generate mid-IR pulses around 1400 cm^{-1}. After the sample, the mid-IR pulses are spectrally dispersed (Chromex 250IS, Bruker) and detected with a double 64 channel MCT array (IR-0144, Infrared Systems Development). The energy of the excitation pulses was ca. 500 nJ (diameter at the sample position ca. 200 µm). In order to prevent nonlinearities from multistep or multiphoton excitation, the excitation intensity was reduced by stretching the excitation pulses by propagation through a 25 cm rod of fused silica. This resulted in a duration of the excitation pulse of ca. 1.5 ps. For each setting of the delay time, 1000 shots were averaged. In addition, the data was averaged over 10 scans of the delay line. In addition, averaging over 5 points along the time axis was used to reduce electronic noise. Magic angle conditions and room-temperature were used.

4.2.4 | Details of Sample Properties and Data Handling

In the time-resolved absorption experiments, the Cu(I) samples were dissolved in acetonitrile or dichloromethane purified by distillation from CaH_2 and were kept in a nitrogen atmosphere. The solution (concentration 1,6 mM, total volume ca. 10 cm^3) was pumped with a peristaltic pump (Ismatec, ISM404B) through the cuvette with fused silica windows (UV–vis experiments, optical path length 1 mm for 400 nm excitation or 0.5 mm for 320 nm excitation). For the IR-experiments, CaF_2 windows and pathlengths in the 0.1 mm range were used. The pump speed was set to allow the complete exchange of the irradiated sample volume prior to the next probe pulse. Stationary UV/Vis absorption spectra (UV2600, Shimadzu) were recorded before and after transient measurements to check for the stability of the samples.

In the modeling of the delay time dependence of the transient absorption data, we used global fitting with exponential functions to obtain the relevant time constants and the related amplitude spectra, the decay-associated difference spectra (DADS) (for details, see the Supporting Information of Ref. [25], https://www.nature.com/articles/nchem.2916#Sec9).

4.3 | Fluorescence and Time-Resolved Fluorescence Setup

For the steady-state and time-resolved fluorescence experiments, the excitation wavelength $\lambda_{ex} = 375$ nm with a repetition rate of 5 MHz was obtained from a diode laser (LDH-P-C-375, PicoQuant). Time-correlated single photon counting (TCSPC) was used to record the time decay profiles. The samples were excited after focusing the laser beam with a fused silica lens on a Suprasil quartz glass cuvette (Hellma Analytics, Germany). Selection of the emission wavelength at $\lambda_{em} = 554$ nm was achieved by using a scanning monochromator with a 1200 g/mm grating blazed at 510 nm (2035, McPherson, United States). The monochromator was connected to a hybrid photomultiplier detector assembly (PMA hybrid series 06, PicoQuant, Germany) which is sensitive in the range of 220–650 nm. This detector was connected to a single photon counting PCI express card (TimeHarp260P, PicoQuant, Germany). The resolution was 0.05 ns. Emission spectra were measured in the same setup and recorded with a spectrometer (QE65000, Ocean Optics Inc., USA). The experiments were conducted in a cleanroom with constant temperature

(22.0°C ± 0.5°C) and humidity (40% ± 3%). To analyze the obtained data, the same procedure as in [2] was used.

4.4 | Density Functional Theory

In extensive benchmarking studies [80, 86–89], we found that the structures of TMGqu copper bis(chelate) complexes are well described by the hybrid functionals B3LYP [90–93] and TPSSh [94, 95] with the triple-zeta basis set def2-tzvp [96–99]. The starting geometries of the complexes for the optimization were generated from the X-ray crystal structures. However, the calculation of excited singlets were performed with the functional B3LYP with the keyword "Opt=(MaxStep=10) freq td=(nstates=xx,root=yy,read)" in analogy to the previous publication [25]. The triple-zeta basis set allowed no successful iterations within 2 months of calculation time on 16 nodes. Hence, we stepped back to def2-svp as basis set [93–99]. For all calculations, Gaussian 16 revision B.01 was used [100]. For B3LYP/def2-svp, the key geometric data of the symmetry-allowed singlet excitations are summarized in Table 2. The triplet state T_1 can be handled as pseudo ground state.

Acknowledgments

S.H.-P. and M.R. acknowledge financial support by the Deutsche Forschungsgemeinschaft (FOR1405 and 413524714). Moreover, W.Z. thanks the SFB749 (project A5) and the Cluster of Excellence "Munich-Center for Advanced Photonics" and "Center for Integrated Protein Science (CIPSM)." We furthermore thank the Paderborn Center for Parallel Computing, PC^2, for providing computing time on the High-Performance Computing (HPC) system OCuLUS as well as support.

Open Access funding enabled and organized by Projekt DEAL.

Conflicts of Interest

The authors declare no conflicts of interest.

Data Availability Statement

The data that support the findings of this study are available from the corresponding author, S.H,-P., upon reasonable request.

References

1. L. Bergmann, G. J. Hedley, T. Baumann, S. Bräse, and I. D. W. Samuel, "Direct Observation of Intersystem Crossing in a Thermally Activated Delayed Fluorescence Copper Complex in the Solid State," *Science Advances* 2 (2016): e1500889.

2. B. Kumar, M. Llorente, J. Froehlich, T. Dang, A. Sathrum, and C. P. Kubiak, "Photochemical and Photoelectrochemical Reduction of CO_2," *Annual Review of Physical Chemistry* 63 (2012): 541–569.

3. Z. A. Siddique, Y. Yamamoto, T. Ohno, and K. Nozaki, "Structure-Dependent Photophysical Properties of Singlet and Triplet Metal-to-Ligand Charge Transfer States in Copper(I) Bis(diimine) Compounds," *Inorganic Chemistry* 42 (2003): 6366–6378.

4. L. X. Chen, G. B. Shaw, I. Novozhilova, et al., "MLCT State Structure and Dynamics of a Copper(I) Diimine Complex Characterized by Pump−Probe X-Ray and Laser Spectroscopies and DFT Calculations," *Journal of the American Chemical Society* 125 (2003): 7022–7034.

5. I. O. Koshevoy, M. Krause, and A. Klein, "Non-Covalent Intramolecular Interactions through Ligand-Design Promoting Efficient Photoluminescence from Transition Metal Complexes," *Coordination Chemistry Reviews* 405 (2020): 213094.

6. L. H. M. de Groot, A. Ilic, J. Schwarz, and K. Wärnmark, "Iron Photoredox Catalysis–Past, Present, and Future," *Journal of the American Chemical Society* 145 (2023): 9369–9388.

7. A. Y. Chan, A. Ghosh, J. T. Yarranton, et al., "Exploiting the Marcus Inverted Region for First-Row Transition Metal–based Photoredox Catalysis," *Science* 382 (2023): 191–197.

8. J. K. McCusker, "Electronic Structure in the Transition Metal Block and Its Implications for Light Harvesting," *Science* 363 (2019): 484–488.

9. S. Garakyaraghi, C. E. McCusker, S. Khan, P. Koutnik, A. T. Bui, and F. N. Castellano, "Enhancing the Visible-Light Absorption and Excited-State Properties of Cu(I) MLCT Excited States," *Inorganic Chemistry* 57 (2018): 2296–2307.

10. A. Ghosh, J. T. Yarranton, and J. K. McCusker, "Establishing the Origin of Marcus-Inverted-Region Behaviour in the Excited-State Dynamics of Cobalt(III) Polypyridyl Complexes," *Nature Chemistry* 16 (2024): 1665–1672.

11. D. Bím, K. M. Luedecke, D. A. Cagan, and R. G. Hadt, "Light Activation and Photophysics of a Structurally Constrained Nickel(II)–Bipyridine Aryl Halide Complex," *Inorganic Chemistry* 63 (2024): 4120–4131.

12. L. Kohler, D. Hayes, J. Hong, et al., "Synthesis, Structure, Ultrafast Kinetics, and Light-Induced Dynamics of CuHETPHEN Chromophores," *Dalton Transactions* 45 (2016): 9871–9883.

13. M. W. Mara, N. E. Jackson, J. Huang, et al., "Effects of Electronic and Nuclear Interactions on the Excited-State Properties and Structural Dynamics of Copper(I) Diimine Complexes," *The Journal of Physical Chemistry B* 117 (2013): 1921–1931.

14. R. Giereth, I. Reim, W. Frey, H. Junge, S. Tschierlei, and M. Karnahl, "Remarkably Long-Lived Excited States of Copper Photosensitizers Containing an Extended π-System Based on an Anthracene Moiety," *Sustainable Energy & Fuels* 3 (2019): 692–700.

15. S. Keller, A. Prescimone, M.-G. La Placa, et al., "The Shiny Side of Copper: Bringing Copper(i) Light-Emitting Electrochemical Cells Closer to Application," *RSC Advances* 10 (2020): 22631–22644.

16. L. E. Burmeister, L. J. Groth, P. R. Meinhold, et al., "Photoactive Neutral Three-Coordinate Cu(I) Complexes of Anionic N-Heterocyclic Carbenes," *JACS Au* 5 (2025): 2792–2801.

17. L. Hua, M. Iwamura, S. Takeuchi, and T. Tahara, "The Substituent Effect on the MLCT Excited State Dynamics of Cu(i) Complexes Studied by Femtosecond Time-Resolved Absorption and Observation of Coherent Nuclear Wavepacket Motion," *Physical Chemistry Chemical Physics: PCCP* 17 (2015): 2067–2077.

18. M. Iwamura, H. Watanabe, K. Ishii, S. Takeuchi, and T. Tahara, "Coherent Nuclear Dynamics in Ultrafast Photoinduced Structural Change of Bis(diimine)copper(I) Complex," *Journal of the American Chemical Society* 133 (2011): 7728–7736.

19. D. Hayes, L. Kohler, R. G. Hadt, et al., "Excited State Electron and Energy Relays in Supramolecular Dinuclear Complexes Revealed by Ultrafast Optical and X-Ray Transient Absorption Spectroscopy," *Chemical Science* 9 (2018): 860–875.

20. L. Kohler, R. G. Hadt, D. Hayes, L. X. Chen, and K. L. Mulfort, "Synthesis, Structure, and Excited State Kinetics of Heteroleptic Cu(i) Complexes with a New Sterically Demanding Phenanthroline Ligand," *Dalton Transactions* 46 (2017): 13088–13100.

21. G. D. Stroscio, R. D. Ribson, and R. G. Hadt, "Quantifying Entatic States in Photophysical Processes: Applications to Copper Photosensitizers," *Inorganic Chemistry* 58 (2019): 16800–16817.

22. F. Doettinger, Y. Yang, M.-A. Schmid, W. Frey, M. Karnahl, and S. Tschierlei, "Cross-Coupled Phenyl- and Alkynyl-Based Phenanthrolines and Their Effect on the Photophysical and

Electrochemical Properties of Heteroleptic Cu(I) Photosensitizers," *Inorganic Chemistry* 60 (2021): 5391–5401.

23. M. Iwamura, S. Takeuchi, and T. Tahara, "Ultrafast Excited-State Dynamics of Copper(I) Complexes," *Accounts of Chemical Research* 48 (2015): 782–791.

24. M. W. Mara, K. A. Fransted, and L. X. Chen, "Interplays of Excited State Structures and Dynamics in Copper(I) Diimine Complexes: Implications and Perspectives," *Coordination Chemistry Reviews* 282 (2015): 2–18.

25. B. Dicke, A. Hoffmann, J. Stanek, et al., "Transferring the Entatic-State Principle to Copper Photochemistry," *Nature Chemistry* 10 (2018): 355–362.

26. B. L. Vallee and R. J. P. Williams, "Metalloenzymes: the Entatic Nature of Their Active Sites.," *Proceedings of the National Academy of Sciences* 59 (1968): 498–505.

27. R. J. P. Williams, "Catalysis by Metallo-Enzymes: The Entatic State," *Inorganica Chimica Acta Reviews* 5 (1971): 137–155.

28. R. J. P. Williams, "Energised (entatic) States of Groups and of Secondary Structures in Proteins and Metalloproteins," *European Journal of Biochemistry* 234 (1995): 363–381.

29. D. F. Schrempp, S. Leingang, M. Schnurr, E. Kaifer, H. Wadepohl, and H.-J. Himmel, "Inter- and Intramolecular Electron Transfer in Copper Complexes: Electronic Entatic State with Redox-Active Guanidine Ligands," *Chemistry – A European Journal* 23 (2017): 13607–13611.

30. D. F. Schrempp, E. Kaifer, and H.-J. Himmel, "Solvent Control of Ligand–Metal Electron Transfer in Mononuclear Copper Complexes with Redox-Active Bisguanidine Ligands," *European Journal of Inorganic Chemistry* 2018 (2018): 3660–3667.

31. J. Stanek, A. Hoffmann, and S. Herres-Pawlis, "Renaissance of the Entatic State Principle," *Coordination Chemistry Reviews* 365 (2018): 103–121.

32. E. W. Dahl and N. K. Szymczak, "Hydrogen Bonds Dictate the Coordination Geometry of Copper: Characterization of a Square-Planar Copper(I) Complex," *Angewandte Chemie International Edition* 55 (2016): 3101–3105.

33. L. Garcia, F. Cisnetti, N. Gillet, et al., "Entasis through Hook-and-Loop Fastening in a Glycoligand with Cumulative Weak Forces Stabilizing Cu^{I}," *Journal of the American Chemical Society* 137 (2015): 1141–1146.

34. P. Comba, S. Fukuzumi, C. Koke, B. Martin, A.-M. Löhr, and J. Straub, "A Bispidine Iron(IV)–Oxo Complex in the Entatic State," *Angewandte Chemie International Edition* 55 (2016): 11129–11133.

35. C. Kieninger, E. Deery, A. D. Lawrence, et al., "The Hydrogenobyric Acid Structure Reveals the Corrin Ligand as an Entatic State Module Empowering B_{12} Cofactors for Catalysis," *Angewandte Chemie International Edition* 58 (2019): 10756–10760.

36. T. Seitz, A. Karabulut, R. M. Suzuki, J. Heck, A. Hoffmann, and S. Herres-Pawlis, *Chem. Commun*. (2025).

37. B. G. Malmstrom, "Rack-induced Bonding in Blue-copper Proteins," *European Journal of Biochemistry* 223 (1994): 711–718.

38. E. I. Solomon and R. G. Hadt, "Recent Advances in Understanding Blue Copper Proteins," *Coordination Chemistry Reviews* 255 (2011): 774–789.

39. H. B. Gray and B. G. Malmstroem, "Long-Range Electron Transfer in Multisite Metalloproteins," *Biochemistry* 28 (1989): 7499–7505.

40. W. R. Hagen, "Hypothesis: Entatic *versus* Ecstatic States in Metalloproteins," *Metallomics: Integrated Biometal Science* 11 (2019): 1768–1778.

41. P. Comba, "Coordination Compounds in the Entatic State," *Coordination Chemistry Reviews* 200–202 (2000): 217–245.

42. P. Comba and W. Schiek, "Fit and Misfit between Ligands and Metal Ions," *Coordination Chemistry Reviews* 238-239 (2003): 21–29.

43. P. Comba, "Strains and Stresses in Coordination Compounds," *Coordination Chemistry Reviews* 182 (1999): 343–371.

44. A. Hoffmann, S. Binder, A. Jesser, et al., "Catching an Entatic State—A Pair of Copper Complexes," *Angewandte Chemie International Edition* 53 (2014): 299–304.

45. P. R. Raithby, G. P. Shields, F. H. Allen, and W. D. S. Motherwell, "Structure Correlation Study of Four-Coordinate Copper(I) and (II) Complexes," *Acta Crystallographica Section B Structural Science* 56 (2000): 444–454.

46. J. Stanek, T. Rösener, A. Metz, J. Mannsperger, A. Hoffmann, and S. Herres-Pawlis, in *Guanidines as Reagents and Catalysts II*, 2015, pp. 95–164.

47. D. Petrovic, L. M. Hill, P. G. Jones, W. B. Tolman, and M. Tamm, "Synthesis and Reactivity of Copper(i) Complexes with an Ethylene-Bridged Bis(imidazolin-2-Imine) Ligand," *Dalton Transactions*. (2008): 887–894.

48. O. Bienemann, A. Hoffmann, and S. Herres-Pawlis, "(Guanidine) Copper Complexes: Structural Variety and Application in Bioinorganic Chemistry and Catalysis," *Reviews in Inorganic Chemistry* (2011): 83–108.

49. S. Herres-Pawlis, G. Wellenreuther, A. Eich, et al., "Stabilisation of a Highly Reactive Bis(μ-oxo)dicopper(III) Species at Room Temperature by Electronic and Steric Constraint of an Unconventional Nitrogen Donor Ligand," *Chemistry – A European Journal* 15 (2009): 8678–8682.

50. D. Maiti, D.-H. Lee, K. Gaoutchenova, et al., "Reactions of a Copper(II) Superoxo Complex Lead to C-H and O-H Substrate Oxygenation: Modeling Copper-Monooxygenase C-H Hydroxylation," *Angewandte Chemie* 120 (2008): 88–91.

51. M. Schatz, V. Raab, S. P. Foxon, et al., "Spektroskopischer Und Theoretischer Nachweis Eines beständigen End-on-Kupfersuperoxokomplexes," *Angewandte Chemie* 116 (2004): 4460–4464.

52. C. Würtele, E. Gaoutchenova, K. Harms, M. C. Holthausen, J. Sundermeyer, and S. Schindler, "Kristallographische Charakterisierung Eines Synthetischen 1:1-End-on-Kupferdisauerstoff- Adduktkomplexes," *Angewandte Chemie* 118 (2006): 3951–3954.

53. I. Shimizu, Y. Morimoto, D. Faltermeier, et al., "Tetrahedral Copper(II) Complexes with a Labile Coordination Site Supported by a Tris-Tetramethylguanidinato Ligand," *Inorganic Chemistry* 56 (2017): 9634–9645.

54. M. Paul, M. Teubner, B. Grimm-Lebsanft, et al., "Exceptional Substrate Diversity in Oxygenation Reactions Catalyzed by a Bis(μ-oxo) Copper Complex," *Chemistry – A European Journal* 26 (2020): 7556–7562.

55. J. S. Woertink, L. Tian, D. Maiti, et al., "Spectroscopic and Computational Studies of an End-on Bound Superoxo-Cu(II) Complex: Geometric and Electronic Factors That Determine the Ground State," *Inorganic Chemistry* 49 (2010): 9450–9459.

56. D. Maiti, D.-H. Lee, A. A. N. Sarjeant, et al., "Reaction of a Copper−Dioxygen Complex with Nitrogen Monoxide (•NO) Leads to a Copper(II)−Peroxynitrite Species," *Journal of the American Chemical Society* 130 (2008): 6700–6701.

57. C. Saracini, D. G. Liakos, J. E. Z. Rivera, F. Neese, G. J. Meyer, and K. D. Karlin, "Excitation Wavelength Dependent O_2 Release from Copper(II)–Superoxide Compounds: Laser Flash-Photolysis Experiments and Theoretical Studies," *Journal of the American Chemical Society* 136 (2014): 1260–1263.

58. A. Metz, J. Heck, C. M. Gohlke, et al., "Reactivity of Zinc Halide Complexes Containing Camphor-Derived Guanidine Ligands with Technical Rac-Lactide," *Inorganics* 5 (2017): 85.

59. A. Metz, R. Plothe, B. Glowacki, et al., "Zinc Chloride Complexes with Aliphatic and Aromatic Guanidine Hybrid Ligands and Their Activity in the Ring-Opening Polymerisation of d,l -Lactide," *European Journal of Inorganic Chemistry* 2016 (2016): 4974–4987.

60. I. dos Santos Vieira and S. Herres-Pawlis, "Lactide Polymerisation with Complexes of Neutral N-Donors – New Strategies for Robust Catalysts," *European Journal of Inorganic Chemistry* 2012 (2012): 765–774.

61. A. Brar and S. Kaur, "Tetramethylguanidino-tris(2-aminoethyl)amine: A Novel Ligand for Copper-based Atom Transfer Radical Polymerization," *Journal of Polymer Science Part A: Polymer Chemistry* 43 (2005): 5906–5922.

62. O. Bienemann, R. Haase, A. Jesser, et al., "Synthesis and Application of New Guanidine Copper Complexes in Atom Transfer Radical Polymerisation," *European Journal of Inorganic Chemistry* 2011 (2011): 2367–2379.

63. T. Rösener, O. Bienemann, K. Sigl, et al., "A Comprehensive Study of Copper Guanidine Quinoline Complexes: Predicting the Activity of Catalysts in ATRP with DFT," *Chemistry – A European Journal* 22 (2016): 13550–13562.

64. T. Rösener, K. Kröckert, A. Hoffmann, and S. Herres-Pawlis, "The Curious Case of a Phenylated Guanidinoquinoline Ligand: Synthesis, Complexes and ATRP Properties of DMEG6phqu," *Zeitschrift für anorganische und allgemeine Chemie* 644 (2018): 1317–1328.

65. K. W. Kröckert, J. S. Mannsperger, T. Rösener, A. Hoffmann, and S. Herres-Pawlis, "Increasing the Activity of Copper Guanidine Quinoline Catalysts: Substitution at the Quinoline Backbone Leads to Highly Active Complexes for ATRP," *Zeitschrift für anorganische und allgemeine Chemie* 647 (2021): 832–842.

66. A. Hoffmann, O. Bienemann, I. dos Santos Vieira, and S. Herres-Pawlis, "New Guanidine-Pyridine Copper Complexes and Their Application in ATRP," *Polymers* 6 (2014): 995–1007.

67. T. Becker, A. Hermann, N. Saritas, A. Hoffmann, and S. Herres-Pawlis, "Open- and Closed-Loop Recycling: Highly Active Zinc Bisguanidine Polymerization Catalyst for the Depolymerization of Polyesters," *ChemSusChem* 17 (2024): e202400933.

68. M. Fuchs, P. M. Schäfer, W. Wagner, et al., "A Multitool for Circular Economy: Fast Ring-Opening Polymerization and Chemical Recycling of (Bio)polyesters Using a Single Aliphatic Guanidine Carboxy Zinc Catalyst," *ChemSusChem* 16 (2023): e202300192.

69. M. H. Vos and U. Liebl, "Time-Resolved Infrared Spectroscopic Studies of Ligand Dynamics in the Active Site from Cytochrome c Oxidase," *Biochimica et Biophysica Acta (BBA) – Bioenergetics* 1847 (2015): 79–85.

70. D. B. Bucher, B. M. Pilles, T. Carell, and W. Zinth, "Charge Separation and Charge Delocalization Identified in Long-Living States of Photoexcited DNA," *Proceedings of the National Academy of Sciences* 111 (2014): 4369–4374.

71. F. E. Poynton, J. P. Hall, P. M. Keane, et al., "Direct Observation by Time-Resolved Infrared Spectroscopy of the Bright and the Dark Excited States of the $[Ru(phen)_2\ (dppz)]^{2+}$ Light-Switch Compound in Solution and when Bound to DNA," *Chemical Science* 7 (2016): 3075–3084.

72. P. Hamm, S. M. Ohline, and W. Zinth, "Vibrational Cooling after Ultrafast Photoisomerization of Azobenzene Measured by Femtosecond Infrared Spectroscopy," *The Journal of Chemical Physics* 106 (1997): 519–529.

73. J. Chaudhuri, S. Kume, J. Jagur-Grodzinski, and M. Szwarc, "Chemistry of Radical Anions of Heterocyclic Aromatics. I. Electron Spin Resonance and Electronic Spectra," *Journal of the American Chemical Society* 90 (1968): 6421–6425.

74. Y. Zhang, M. Schulz, M. Wächtler, M. Karnahl, and B. Dietzek, "Heteroleptic Diimine–diphosphine Cu(I) Complexes as an Alternative towards Noble-Metal Based Photosensitizers: Design Strategies, Photophysical Properties and Perspective Applications," *Coordination Chemistry Reviews* 356 (2018): 127–146.

75. D. G. Cuttell, S.-M. Kuang, P. E. Fanwick, D. R. McMillin, and R. A. Walton, "Simple Cu(I) Complexes with Unprecedented Excited-State Lifetimes," *Journal of the American Chemical Society* 124 (2002): 6–7.

76. A. Hoffmann, J. Stanek, B. Dicke, et al., "Implications of Guanidine Substitution on Copper Complexes as Entatic-State Models," *European Journal of Inorganic Chemistry* 2016 (2016): 4731–4743.

77. M. Kasha, "Characterization of Electronic Transitions in Complex Molecules," *Discussions of the Faraday Society* 9 (1950): 14–19.

78. J. Stanek, N. Sackers, F. Fink, et al., "Copper Guanidinoquinoline Complexes as Entatic State Models of Electron-Transfer Proteins," *Chemistry – A European Journal* 23 (2017): 15738–15745.

79. J. Stanek, M. Konrad, J. Mannsperger, A. Hoffmann, and S. Herres-Pawlis, "Influence of Functionalized Substituents on the Electron-Transfer Abilities of Copper Guanidinoquinoline Complexes," *European Journal of Inorganic Chemistry* 2018 (2018): 4997–5006.

80. A. Hoffmann, M. Rohrmüller, A. Jesser, I. dos Santos Vieira, W. G. Schmidt, and S. Herres-Pawlis, "Geometrical and Optical Benchmarking of Copper(II) Guanidine–quinoline Complexes: Insights from TD-DFT and Many-body Perturbation Theory (part II)," *Journal of Computational Chemistry* 35 (2014): 2146–2161.

81. M. Dittmann, F. F. Graupner, B. Maerz, et al., "Photostability of 4,4′-Dihydroxythioindigo, a Mimetic of Indigo," *Angewandte Chemie International Edition* 53 (2014): 591–594.

82. E. Riedle, M. Beutter, S. Lochbrunner, et al., "Generation of 10 to 50 fs Pulses Tunable through All of the Visible and the NIR," *Applied Physics B* 71 (2000): 457–465.

83. R. Huber, H. Satzger, W. Zinth, and J. Wachtveitl, "Noncollinear Optical Parametric Amplifiers with Output Parameters Improved by the Application of a White Light Continuum Generated in CaF2," *Optics Communications* 194 (2001): 443–448.

84. P. N. Dominguez, M. Himmelstoss, J. Michelmann, et al., "Primary Reactions in Photosynthetic Reaction Centers of Rhodobacter Sphaeroides – Time Constants of the Initial Electron Transfer," *Chemical Physics Letters* 601 (2014): 103–109.

85. S. Schmidt, T. Arlt, P. Hamm, et al., "Primary Electron-Transfer Dynamics in Modified Bacterial Reaction Centers Containing Pheophytin-a Instead of Bacteriopheophytin-a," *Spectrochimica Acta Part A: Molecular and Biomolecular Spectroscopy* 51 (1995): 1565–1578.

86. A. Jesser, M. Rohrmüller, W. G. Schmidt, and S. Herres-Pawlis, "Geometrical and Optical Benchmarking of Copper Guanidine–quinoline Complexes: Insights from TD-DFT and Many-body Perturbation Theory †," *Journal of Computational Chemistry* 35 (2014): 1–17.

87. A. Hoffmann, R. Grunzke, and S. Herres-Pawlis, "Insights into the Influence of Dispersion Correction in the Theoretical Treatment of Guanidine-Quinoline Copper(I) Complexes," *Journal of Computational Chemistry* 35 (2014): 1943–1950.

88. M. Rohrmüller, A. Hoffmann, C. Thierfelder, S. Herres-Pawlis, and W. G. Schmidt, "The Cu_2O_2 Torture Track for a Real-Life System: $[Cu_2\ (btmgp)_2O_2]^{2+}$ Oxo and Peroxo Species in Density Functional Calculations," *Journal of Computational Chemistry* 36 (2015): 1672–1685.

89. M. Rohrmüller, S. Herres-Pawlis, M. Witte, and W. G. Schmidt, "Bis-μ-oxo and μ-$\eta^{\ 2}$:$\eta^{\ 2}$-peroxo Dicopper Complexes Studied Within (time-dependent) Density-functional and Many-body Perturbation Theory," *Journal of Computational Chemistry* 34 (2013): 1035–1045.

90. C. Lee, W. Yang, and R. G. Parr, "Development of the Colle-Salvetti Correlation-Energy Formula into a Functional of the Electron Density," *Physical Review B* 37 (1988): 785–789.

91. B. Miehlich, A. Savin, H. Stoll, and H. Preuss, "Results Obtained with the Correlation Energy Density Functionals of Becke and Lee, Yang and Parr," *Chemical Physics Letters* 157 (1989): 200–206.

92. P. J. Stephens, F. J. Devlin, C. F. Chabalowski, and M. J. Frisch, "Ab Initio Calculation of Vibrational Absorption and Circular Dichroism Spectra Using Density Functional Force Fields," *The Journal of Physical Chemistry* 98 (1994): 11623–11627.

93. C. Adamo and V. Barone, "Toward Reliable Density Functional Methods without Adjustable Parameters: The PBE0 Model," *The Journal of Chemical Physics* 110 (1999): 6158–6170.

94. J. Tao, J. P. Perdew, V. N. Staroverov, and G. E. Scuseria, "Climbing the Density Functional Ladder: Nonempirical Meta–Generalized Gradient Approximation Designed for Molecules and Solids," *Physical Review Letters* 91 (2003): 146401.

95. V. N. Staroverov, G. E. Scuseria, J. Tao, and J. P. Perdew, "Comparative Assessment of a New Nonempirical Density Functional: Molecules and Hydrogen-Bonded Complexes," *The Journal of Chemical Physics* 119 (2003): 12129–12137.

96. K. Eichkorn, F. Weigend, O. Treutler, and R. Ahlrichs, "Auxiliary Basis Sets for Main Row Atoms and Transition Metals and Their use to Approximate Coulomb Potentials," *Theoretical Chemistry Accounts: Theory, Computation, and Modeling (Theoretica Chimica Acta)* 97 (1997): 119–124.

97. F. Weigend, M. Häser, H. Patzelt, and R. Ahlrichs, "RI-MP2: Optimized Auxiliary Basis Sets and Demonstration of Efficiency," *Chemical Physics Letters* 294 (1998): 143–152.

98. F. Weigend and R. Ahlrichs, "Balanced Basis Sets of Split Valence, Triple Zeta Valence and Quadruple Zeta Valence Quality for H to Rn: Design and Assessment of Accuracy," *Physical Chemistry Chemical Physics: PCCP* 7 (2005): 3297–3305.

99. A. Schäfer, C. Huber, and R. Ahlrichs, "Fully Optimized Contracted Gaussian Basis Sets of Triple Zeta Valence Quality for Atoms Li to Kr," *The Journal of Chemical Physics* 100 (1994): 5829–5835.

100. M. J. Frisch, G. W. Trucks, H. B. Schlegel, et al., *Gaussian 16, revision B.01* (Wallington, CT: Gaussian Inc., 2016).

Supporting Information

Additional supporting information can be found online in the Supporting Information section.